

CI and CO in nearby galaxy centers

The bright galaxies NGC 1068 (M 77), NGC 2146, NGC 3079, NGC 4826 (M 64), and NGC 7469

F.P. Israel¹

Sterrewacht Leiden, Leiden University, P.O. Box 9513, 2300 RA Leiden, The Netherlands

Received ????: accepted ????

ABSTRACT

Aims. We study the physical properties and amount of molecular gas in the central regions of galaxies with active nuclei.

Methods. Maps and measurements of the $J=1-0$, $J=2-1$, $J=3-2$, $J=4-3$ ^{12}CO , the $J=1-0$, $J=2-1$, and $J=3-2$ ^{13}CO lines in the central arcminute squared of NGC 1068, NGC 2146, NGC 3079, NGC 4826, and NGC 7469, as well as 492 GHz CI maps in three of these are used to model the molecular gas clouds in these galaxies.

Results. Bright CO concentrations were detected and mapped in all five objects. In all cases, the observed lines could be fitted with two distinct gas components. The physical condition of the molecular gas is found to differ from galaxy to galaxy. Rather high kinetic temperatures of 125-150 K occur in NGC 2146 and NGC 3079. Very high densities of $0.3 - 1.0 \times 10^5 \text{ cm}^{-3}$ occur in NGC 2146, NGC 3079, and NGC 7469. The CO to H_2 conversion factor X is typically an order of magnitude less than the ‘standard’ value in the Solar Neighborhood. The molecular gas is constrained within radii between 0.9 and 1.5 kpc from the nuclei. Within these radii, H_2 masses are typically $1.2 - 2.5 \times 10^8 M_{\odot}$. The exception is the (relatively nearby) merger NGC 4826 with $R=0.3$ kpc, and $M = 3 \times 10^7 M_{\odot}$. The H_2 mass is typically about one per cent of the dynamical mass in the same region.

Key words. Galaxies – individual: NGC 1068, NGC 3079, NGC 7469 – ISM – centers; Radio lines – galaxies; ISM – molecules, CO, C° , H_2

1. Introduction

Molecular gas is a major constituent of the interstellar medium in galaxies. This is particularly true for star-forming complexes in the spiral arms, but strong concentrations of molecular gas are also frequently found in the inner few kiloparsec of spiral galaxies. These concentrations of gas play an important role in the evolution of galaxy centers. They provide the material for inner galaxy starbursts and the accretion of massive black holes. It is thus important to determine the characteristics of this molecular hydrogen gas (density, temperature, excitation) and especially its amount. It cannot be observed directly, and its properties can only be inferred from observations of tracer elements, of which CO is one of the most abundant and easiest observable. However, the CO emitting gas is not in LTE, and the most commonly observed ^{12}CO lines are optically thick. We have to observe CO in various transitions to obtain reliable physical results and to break the temperature-density degeneracy that plagues ^{12}CO intensities, also in an optically thin isotope (e.g. also in ^{13}CO). The observed molecular and atomic line intensities then provide the essential input for further modeling.

We have therefore observed a sample of nearby spiral galaxy centers in various CO transitions and in the 492 GHz $^3\text{P}_1-^3\text{P}_0$ [CI] transition. These galaxies were selected to be bright at infrared wavelengths, and more specifically to have IRAS flux densities $f_{12\mu\text{m}} \geq 1.0$ Jy. The results

for seven galaxies from this sample have already been published. These are NGC 253 (Israel et al. 1995), NGC 7331 (Israel & Baas 1999), NGC 6946, and M 83 = NGC 5236 (Israel & Baas 2001 – Paper I), IC 342 and Maffei 2 (Israel & Baas 2003 – Paper II), M 51 = NGC 5194 (Israel et al. 2006 – Paper III). In this paper, we present results obtained for an additional five bright and well-studied galaxies. In Table 1 we have summarized the characteristics of their appearance.

At least three of the galaxies discussed in this paper have an active (Seyfert) nucleus (NGC 1068, NGC 3079, and NGC 7469), and probably also NGC 4826. Two of the galaxies (NGC 2146 and NGC 4826) show evidence of a merger event and all – including most of the galaxies published earlier (IC 342, Maffei 2, M 83, and NGC 6946) – show signs of enhanced star formation activity in the recent past or present. NGC 4826 is as nearby as IC 342, Maffei 2, M 83, and NGC 6946) affording similar linear resolutions of 200–300 pc. The other galaxies are more distant so that our angular resolution of $10'' - 14''$ corresponds to a linear resolution no better than 800-2000 pc. Such low linear resolutions do not reveal much structural detail in the central CO distributions; millimeter array observations are required for this. However, the multi-transition observations of ^{12}CO and ^{13}CO presented here allow us to characterize the overall physical condition of the central molecular gas in ways that are not possible otherwise.

Send offprint requests to: F.P. Israel

Table 1. Galaxy parameters

	NGC 1068	NGC 2146	NGC 3079	NGC 4826	NGC 7469
Type ^a	(R)SA(rs)b; Sy1	SB(s)abp; HII	SB(s)c; Lin; Sy2	(R)SA(rs)ab; HII/Lin	(R)SAB(rs)a; Sy1.2
R.A. (B1950) ^a	02 ^h 40 ^m 07.1 ^s	06 ^h 10 ^m 40.2 ^s	09 ^h 58 ^m 35 ^s	12 ^h 54 ^m 16.3 ^s	23 ^h 00 ^m 44.4 ^s
Decl.(B1950) ^a	-00°13'32"	+78°22'29"	+55°55'16"	+21°57'10.4"	+08°36'16"
R.A. (J2000) ^a	02 ^h 42 ^m 40.7 ^s	06 ^h 18 ^m 37.7 ^s	10 ^h 01 ^m 58 ^s	12 ^h 56 ^m 43.7 ^s	23 ^h 03 ^m 15.6 ^s
Decl.(J2000) ^a	-00°00'48"	+78°21'25"	+55°40'47"	+21°40'58"	+08°52'26"
V_{LSR}^b	+1023 km s ⁻¹	+879 km s ⁻¹	+1116 km s ⁻¹	+408 km s ⁻¹	+4889 km s ⁻¹
Inclination i^b	37°	51°	74°	60°	46°
Position angle P^b	82°	128°	165°	112°	128°
Distance D^c	16.5 Mpc	17.9 Mpc	19.4 Mpc	4.1 Mpc	29.5 Mpc
Scale	80 pc/''	87 pc/''	94 pc/''	20 pc/''	143 pc/''

Notes to Table 1: ^a NED ^b Kaneko et al. (1989); Tarchi et al. (2004); Young et al. (1988b); Irwin & Seaquist (1991); García-Burillo et al. (2003); Beswick, Pedlar & McDonald (2002); Meixner et al. (1990); Davies, Tacconi & Genzel (2004). ^c see Moustakas et al. (2006)

Table 2. ¹²CO observations log

Galaxy	Date	T_{sys} (K)	Beam Size (")	η_{mb}	t(int) (sec)	No. pnts	Map Parameters		
							Size (")	Spacing (")	P.A. (°)
¹² CO $J=1-0$ (115 GHz)									
NGC 1068	07Jan	280	22	0.74	750	1	–	–	–
NGC 2146	05Feb	315			1200	1	–	–	–
NGC 3079	05Oct	264			1680	1	–	–	–
NGC 4826	06Jul	222			840	1	–	–	–
NGC 7469	05Jan	157			960	1	–	–	–
¹² CO $J=2-1$ (230 GHz)									
NGC 1068	07Jan	474	12	0.53	750	1	–	–	–
	94Jan	350	21	0.69	120	71	80×90	7	11
	96Jan	850	21	0.69	120	54	50×90	10	46
NGC 2146	05Feb	290	12	0.53	480	1	–	–	–
	91Apr/93Apr	1420/372	21	0.69	320/300	39	50×80	10	123
NGC 3079	05Oct	352	12	0.53	1200	1	–	–	–
	95Jun	585	21	0.69	240	14	30×30	10	165
NGC 4826	06Jul	331	12	0.53	780	1	–	–	–
	93May/94Jan	570/468	21	0.69	200/300	136	100×80	7	110
NGC 7469	05Jan	224	12	0.53	960	1	–	–	–
	91Sep/00Oct	194/308	21	0.69	400/900	9	30×30	10	35
¹² CO $J=3-2$ (345 GHz)									
NGC 1068	94jan	1180	14	0.58	600	71	70×80	7	45
	96Jan	1980		0.58	120	63	30×63	6	45
NGC 2146	96Jan	1139		0.59	180	28	24×72	8	123
NGC 3079	93Dec	1293		0.56	400	12	14×96	8	165
NGC 4826	93May/94Jan	517/939		0.53	200/480	20	60×30	10	114
NGC 7469	96Jul/01Jun	1358/715		0.61	480/600	32	35×28	7	0
¹² CO $J=4-3$ (461 GHz)									
NGC 1068	96Jul	3365	11	0.50	600	23	24×24	6	45
NGC 2146	01Nov	4743		0.50	1440	4	18×18	6	123
NGC 3079	93Dec/94Mar	3360/5510		0.50	600	13	24×56	8	165
NGC 4826	93Dec/94Mar	2045/4630		0.50	320/600	16	30×60	10	114
NGC 7469	99Jul	2008		0.52	1200	9	18×18	6	0

2. Sample galaxies

2.1. NGC 1068 = Arp 37 = M 77

This is a well-known Seyfert galaxy, relatively luminous at radio wavelengths, with overall and core 1.5 GHz flux densities of 3.8 Jy and 1.1 Jy, respectively (Condon et al.

1990). It has been mapped in HI by Brinks et al. (1997, VLA, 8''), in the $J=1-0$ ¹²CO transition by Scoville et al. (1983; FCRAO, 45''), Young et al. (1995; FCRAO, 45''), Kaneko et al. (1989; Nobeyama, 17''), Helfer et al. (2003, BIMA, 9'' × 6''), in the $J=1-0$ and $J=2-1$ ¹²CO transitions by Planesas et al. (1989; IRAM, 22'', 13'') as well

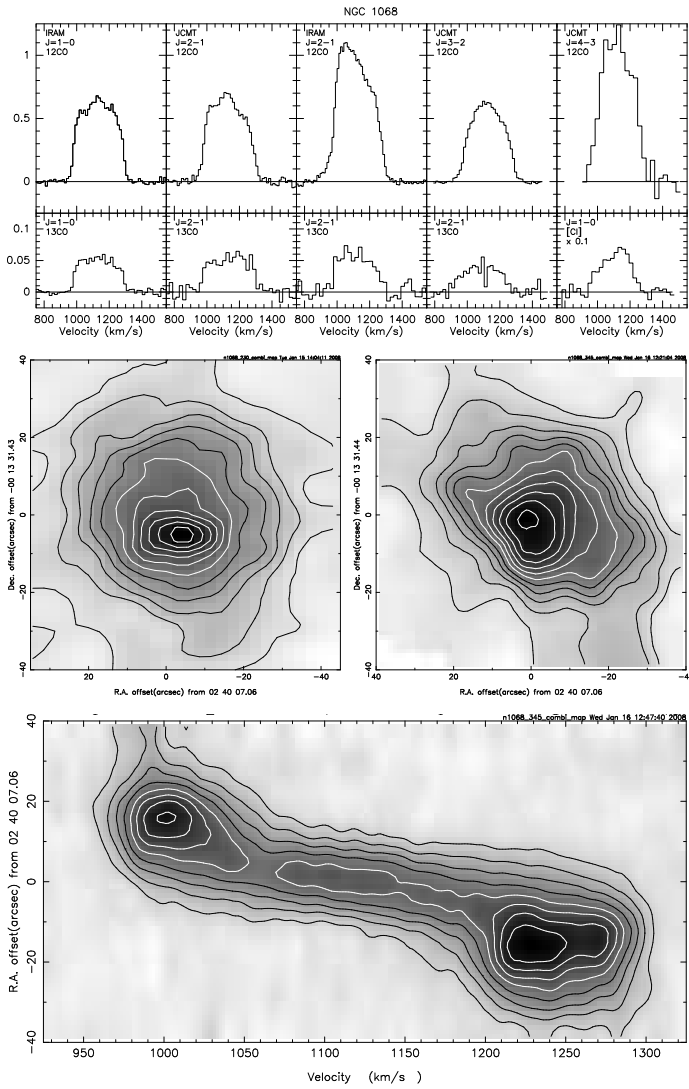


Fig. 1. CO in the center of NGC 1068. Top: Observed line profiles. Horizontal scale is LSR velocity V_{LSR} in km/sec. Vertical scale is main-beam brightness temperature T_{mb} in Kelvins, using the efficiencies listed in Table 2. Note different scales for ^{12}CO , ^{13}CO and [CI] respectively. Center: (Left) $J=2-1$ ^{12}CO emission integrated over the velocity interval 950-1350 km s^{-1} ; contours are in steps of 20 K km s^{-1} ; here and in all other figures, the first contour is equal to the step value. (Right) $J=3-2$ ^{12}CO emission integrated over the same velocity interval; contours step is 15 K km s^{-1} . Bottom: $J=3-2$ ^{12}CO ; position-velocity map in position angle $\text{PA} = 90^\circ$ integrated over a strip $20''$ wide with contours in steps of 0.1 K; east is at top.

as in the $J=2-1$ and $J=3-2$ transitions of both ^{12}CO and ^{13}CO by Papadopoulos & Seaquist (1999; JCMT, $22''$, $14''$). All maps covered more or less the same area that we have mapped, and show only limited detail. The presence of significant structure at angular sizes substantially smaller than these beam sizes was first suggested by Scoville et al (1983), using a daring deconvolution scheme. This was later confirmed by the $J=1-0$ ^{12}CO millimeter array maps made at much higher angular resolutions by Planesas et al. (1991, OVRO, $\approx 3''$), Kaneko et al. (1992, NMA, $\approx 5''$) and in particular the $J=1-0$ ^{12}CO and ^{13}CO maps by Helfer & Blitz (1995, BIMA, $\approx 4''$) and the $J=1-0$ and $J=2-1$ ^{12}CO

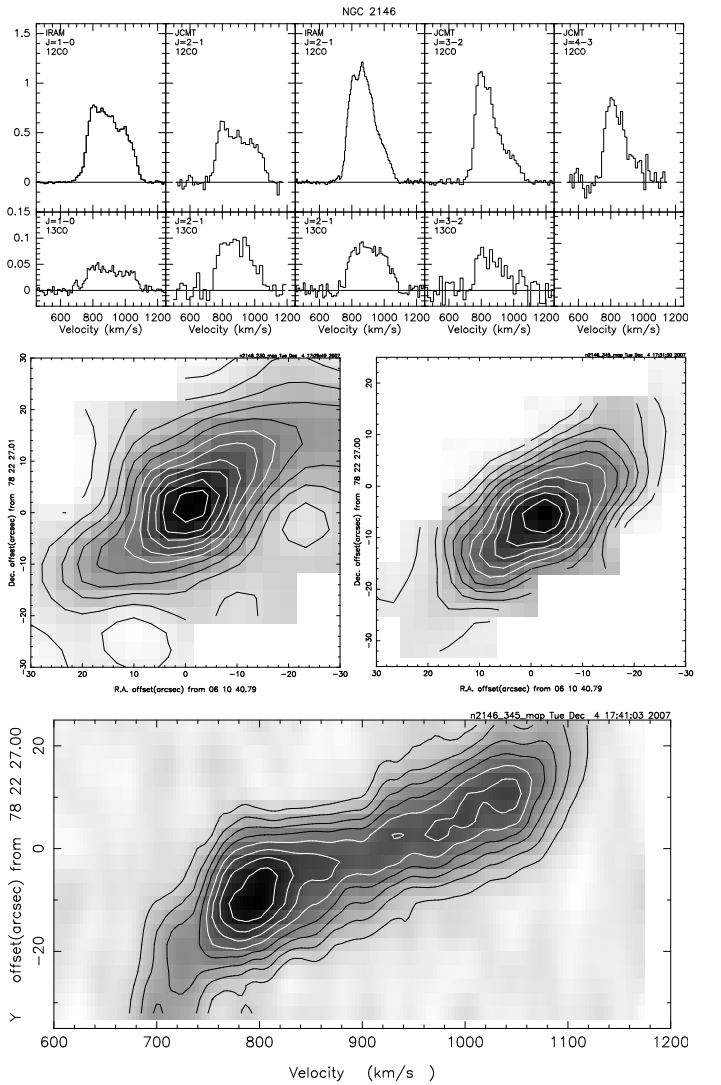


Fig. 2. Center of NGC 2146, as Figure 1. Top: Observed line profiles. Center: (Left) $J=2-1$ ^{12}CO emission integrated over the velocity interval 600-1200 km s^{-1} ; contours step is 15 K km s^{-1} ; (Right) $J=3-2$ ^{12}CO emission integrated over the same velocity interval; contour step is 20 K km s^{-1} . Bottom: $J=3-2$ ^{12}CO ; position-velocity map in position angle $\text{PA} = 303^\circ$ integrated over a strip $20''$ wide with contours in steps of 0.1 K; northwest is at top.

maps by Schinnerer et al. (2000, IRAM, $0.7''$). These show a compact (size about $5''$ or 400 pc) circumnuclear source of molecular line emission, and bright emission extending to about $15''$ (1200 pc) from the nucleus. In lower-resolution maps this emission fortuitously resembles a ring, but higher resolutions clearly reveal CO-bright spiral arms (*cf* Helfer & Blitz 1995). The arms dominate the ^{12}CO emission, but only in the lower J transitions. The interferometer map by Helfer & Blitz (1995) shows strong $J=1-0$ ^{13}CO emission from the arms, but nothing from the nucleus. The compact nucleus cannot be unambiguously identified in the $J=3-2$ ^{13}CO map measured by Papadopoulos & Seaquist (1999) either. The nucleus is also dominant in the light of other molecules (*cf* Jackson et al. 1993, Tacconi et al. 1994; Helfer & Blitz 1995; Usero et al. 2004) that trace high densities or high excitation.

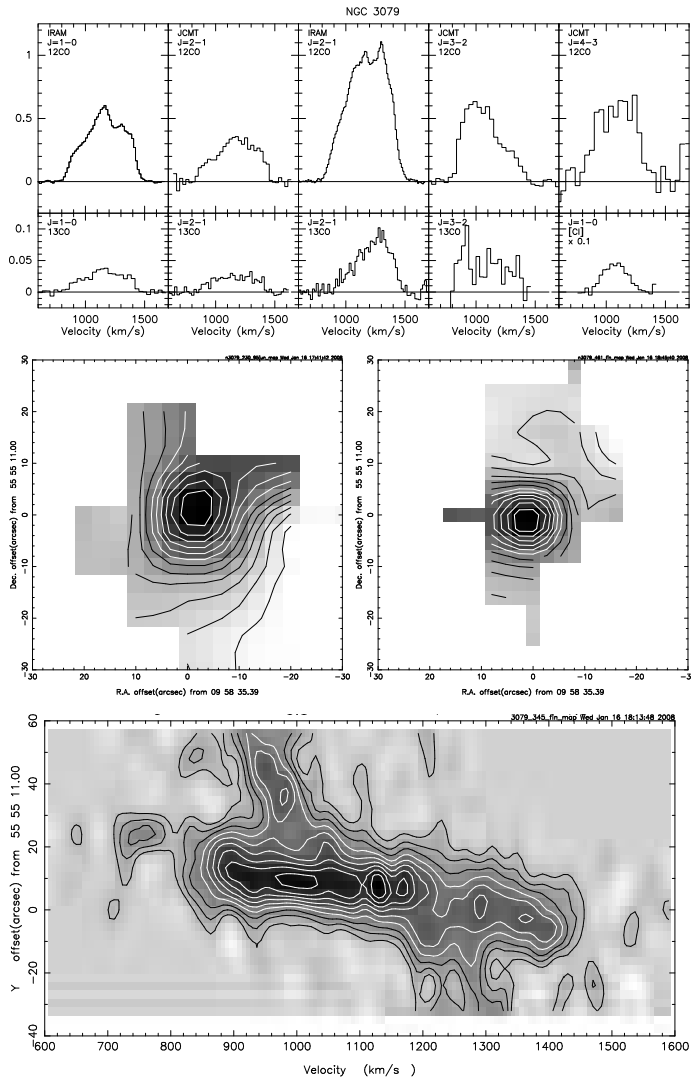


Fig. 3. Center of NGC 3079, as Figure 1. Top: Observed line profiles. Center: (Left) $J=2-1$ ^{12}CO emission integrated over the velocity interval 950-1350 km s^{-1} ; contour step is 15 K km s^{-1} ; (Right) $J=4-3$ ^{12}CO emission integrated over the same velocity interval; contour step is 20 K km s^{-1} . Bottom: $J=3-2$ ^{12}CO ; position-velocity map in position angle $\text{PA} = -11^\circ$ integrated over a strip $20''$ wide with contours in steps of 0.04 K; north is at top.

2.2. NGC 2146

NGC 2146 has an optically disturbed appearance, characterized by a high-surface brightness core crossed by a prominent dust lane, and a number of weaker extraplanar arms and tidal features (see Sandage & Bedke, 1994). This bright core measures several kiloparsecs in diameter, and is a strong source of radio emission (1.4 GHz flux density ≈ 1 Jy, see de Bruyn 1977; Condon et al. 1996; Braun et al. 2007) against which HI is seen in absorption (Taramopoulos et al. 2001, Tarchi et al. 2004). Taramopoulos et al. (2001) have presented a VLA HI map including short spacings that shows a neutral gas filament extending from the main body of galactic HI to the south over half a degree (160 kpc), as well as a large amount of gas extending out of the galaxy to the north. The HI mass of the central region (inner few arcmin) is about $1.6 \times 10^9 M_\odot$. Taramopoulos et

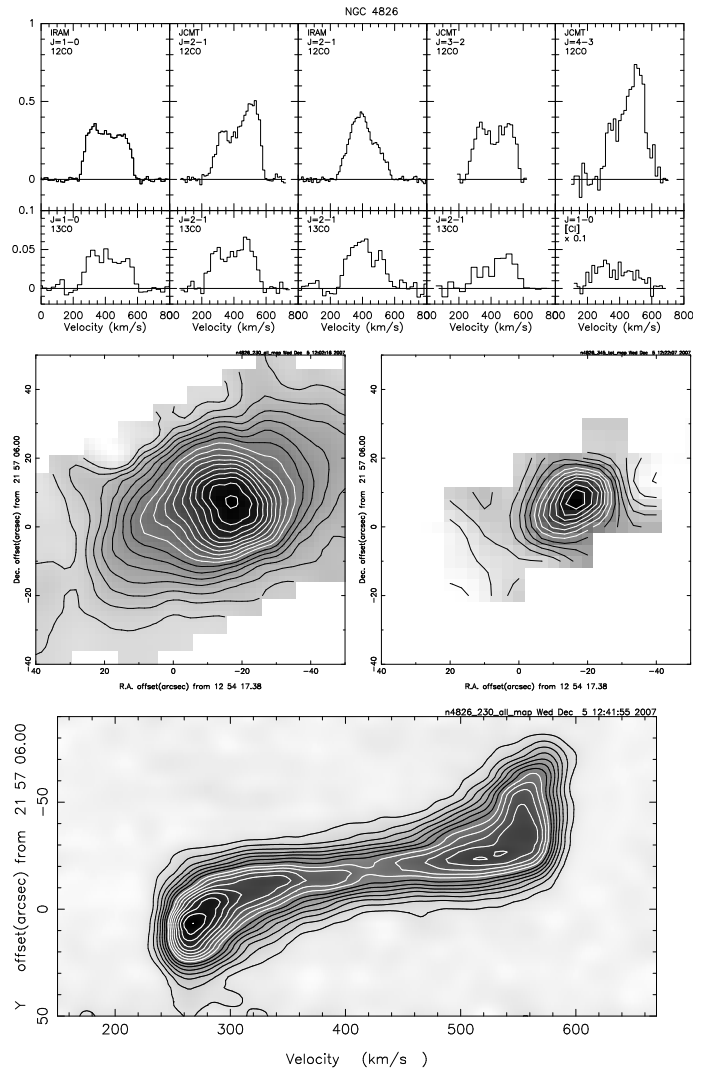


Fig. 4. Center of NGC 4826, as Figure 1. Top: Observed line profiles. Center: (Left) $J=2-1$ ^{12}CO emission integrated over the velocity interval 150-650 km s^{-1} ; contour step is 5 K km s^{-1} ; (Right) $J=3-2$ ^{12}CO emission integrated over the same velocity interval; contour step is 5 K km s^{-1} . Bottom: $J=2-1$ ^{12}CO ; position-velocity map in position angle $\text{PA} = 115^\circ$ integrated over a strip $20''$ wide with contours in steps of 0.03 K; northwest is at top.

al. (2001) conclude that NGC 2146 suffered a merger or close encounter in which the intruder was shredded, about 800 million years ago. The bright core is the site of a powerful starburst. Radio observations reveal numerous supernova remnants, HII regions and water masers throughout (Kronberg & Biermann, 1981; Zhao et al. 1996; Lisenfeld et al. 1996; Tarchi et al. 2000, 2002); a low-luminosity AGN may be present (Inui et al. 2005). X-ray observations also reveal a starburst-driven superwind carrying material away from the galaxy's plane (Armus et al. 1995; Della Ceca et al. 1999). It has been mapped in the $J=1-0$ ^{12}CO line by Young et al. (1988b, FCRAO, $45''$; OVRO, $7''$) and Jackson & Ho (1988, Hat Creek, $6 \times 5''$), in the $J=1-0$ and $J=2-1$ transitions of both ^{12}CO and ^{13}CO by Paglione et al (2001, FCRAO, $45''$) and Xie et al (1994, FCRAO, $23''$) respectively, and in the $J=3-2$ ^{12}CO line by Dumke et al. (2001, HHT, $24''$). The highest resolution observations have

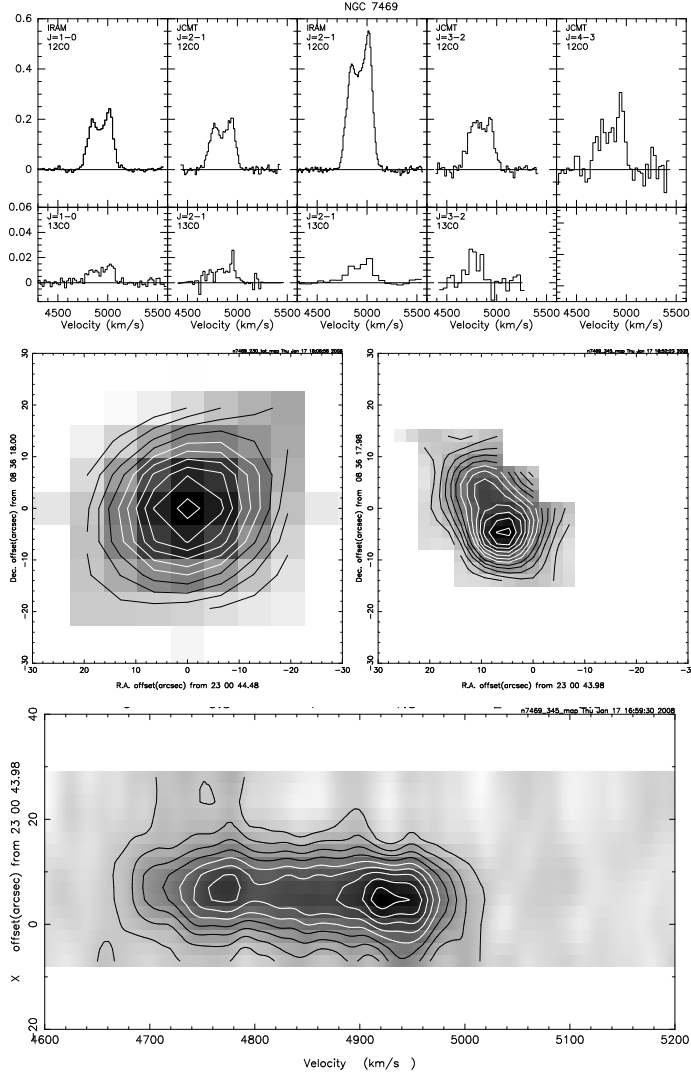


Fig. 5. Center of NGC 7469, as Figure 1. Top: Observed line profiles. Center: (Left) $J=2-1$ ^{12}CO emission integrated over the velocity interval 4650-5050 km s^{-1} ; contour step is 5 K km s^{-1} ; (Right) $J=3-2$ ^{12}CO emission integrated over the same velocity interval; contour step is 7.5 K km s^{-1} . Bottom: $J=3-2$ ^{12}CO ; position-velocity map in position angle $\text{PA} = 128^\circ$ integrated over a strip $20''$ wide with contours in steps of 0.025 K; east is at top.

been published by Greve et al. (2006) using both the IRAM 30 m ($J=1-0$, $J=2-1$ ^{12}CO ; $22''$ and $13''$) and PdB array telescopes ($J=1-0$ ^{12}CO and ^{13}CO ; $J=2-1$ ^{12}CO ; $4-5''$ and $\approx 3''$).

2.3. NGC 3079

This is a large and bright spiral seen almost edge-on. Its central region is a strong source of radio continuum emission (de Bruyn, 1977). It has been mapped in the radio at various resolutions - see references in Condon et al. (1990). These authors list 1.4 GHz flux densities of 0.84 Jy and 0.55 Jy for the whole galaxy and the central region respectively (see also Irwin & Saikia 2003). The center contains a nuclear source (AGN surrounded by water masers, Trotter et al. 1998, Hagiwara et al. 2004) and two wind-driven outflow bubbles (Veilleux et al. 1994; Cecil et al. 2001); it is

Table 3. ^{13}CO and [CI] observations log

Galaxy	Date	T_{sys} (K)	Beam Size ($''$)	η_{mb}	t(int) (sec)
$^{13}\text{CO } J=1-0$ (110 GHz)					
NGC 1068	07Jan	160	23	0.75	1325
NGC 2146	05Feb	153			1200
NGC 3079	05Oct	149			1680
NGC 4826	06Jul	160			1620
NGC 7469	05Jan	121			5760
$^{13}\text{CO } J=2-1$ (220 GHz)					
NGC 1068	96Jan	456	22	0.69	3600
	07Jan	212	13	0.55	1320
NGC 2146	91Sep	1304	22	0.69	3560
	05Feb	374	13	0.55	960
NGC 3079	94Mar	370	22	0.69	5220
	05Oct	374	13	0.55	1200
NGC 4826	93Dec	534	22	0.69	4000
	06Jul	203	13	0.55	780
NGC 7469	95Jun	302	22	0.69	4200
	05Jan	203	13	0.55	1920
$^{13}\text{CO } J=3-2$ (330 GHz)					
NGC 1068	97Nov	427	14	0.59	2400
NGC 2146	01Jan	914		0.59	3600
NGC 3079	95Apr	2637		0.58	1860
NGC 4826	94Apr	1422		0.53	6360
NGC 7469	93Apr	882		0.55	6000
[CI] $^3P_1 - ^3P_0$ (492 GHz)					
NGC 1068 ^a	96Jul	3048	11	0.50	800
NGC 3079 ^b	94Mar	6239		0.50	1200
NGC 4826 ^c	94Dec	2904		0.51	2400
	97Mar	3042		0.51	1200

Notes: ^a Map of 27 points covering $24'' \times 48''$ with spacing $8''$ in $\text{PA} = 70^\circ$. ^b Strip map in declination, 7 points covering $8'' \times 56''$ with spacing $8''$ in $\text{PA} = 165^\circ$. ^c Small 5-point map covering $18'' \times 18''$ with spacing $6''$ in $\text{PA} = 114^\circ$.

a significant X-ray source (Pietsch et al. 1998). The central region also hosts a powerful starburst. In the plane of the galaxy, the cavity surrounding the AGN is marked by near-infrared line emission from shocked H_2 extending out to 300 pc (Israel et al. 1998; see also Hawarden et al. 1994). At the cavity wall, hot dust reaches evaporation temperatures (Israel et al. 1998, see also Armus et al. 1994). Molecular gas has been mapped with a single dish in the $J=1-0$ ^{12}CO line by Tinney et al. (1990, NRAO, $55''$) and Young et al. (1995, FRAO, $45''$), in the $J=1-0$ and $J=2-1$ ^{12}CO lines by Braine et al. (1997), in the $J=1-0$ ^{12}CO and ^{13}CO lines by Paglione et al. (2001, FCRAO $45''$) and with mm arrays in the $J=1-0$ ^{12}CO transition by Young et al. (1988a, OVRO, $8'' \times 6''$), Sofue & Irwin (1992, NMA, $4''$), Tacconi et al. (1996, PdB, $2''$), Sofue et al. (2000, NMA, $1.5''$); Koda et al. (2002, NMA, $1.5''$). HI maps have been presented by Braun et al. (2007). [CI] emission was measured by Gerin & Phillips (2000), and Israel & Baas (2002). Absorption has been mapped in various lines (HI: Pedlar et al. 1996; OH: Hagiwara et al. 2004; CH_3OH : Impellizzeri et al. 2008). All data indicate the presence of dense molecular material extending out to almost a kiloparsec from the nucleus.

2.4. NGC 4826 = M 64

This is a small and nearby early-type (Sab) galaxy. It is relatively isolated although it seems to be part of the loose CVn I group. Its remarkable appearance, with a very prominent and wide dust lane covering the northern edge of its bulge, has caused it to become known as the ‘evil-eye’ galaxy. The discovery (Braun et al. 1992) that its inner parts rotate counter to its outer parts, i.e. that its rotation reverses sign at about $30''$ (600 pc) from the nucleus, has led to considerable interest in this galaxy since. This particular kinematical signature, subsequently studied by Rubin (1994), Walterbos et al. (1994) and Rix et al. (1995), is now generally assumed to mark the acquisition of external material in a merger. It is the outer gas disk that ‘counter-rotates’ (Rix et al. 1995), and the inner gas disk may have contracted from gas that was originally at greater radii but lost much of its angular momentum in the merger (Sil’chenko 1996). The central region is a weak source of radio emission ($S_{1.5GHz} = 100$ mJy). HI maps have been presented by Braun et al. (2007) and Haan et al. (2008) who found a total HI mass $M_{HI} = 1.8 \times 10^8 M_{\odot}$. The galaxy was mapped in ^{12}CO and observed in ^{13}CO in both the $J=1-0$ and the $J=2-1$ transition by Casoli & Gerin (1993), further studied in HI and in $J=3-2$ ^{12}CO by Braun et al. (1994). High-resolution millimeter array observations have been provided in the $J=1-0$ ^{12}CO line by Sakamoto et al. (1999, NMA, $\approx 4''$), in the $J=1-0$ and $J=2-1$ ^{12}CO lines by García-Burillo et al (2003, PdB, $1-3''$) and in the $J=1-0$ ^{12}CO ^{13}CO and HCN lines by Helfer et al. (2003) and Rosolowsky & Blitz (2005).

2.5. NGC 7469 = Arp 298

This is the most distant galaxy in our sample. It is a classical Seyfert 1 galaxy, and it is well-studied at various wavelengths. It appears to be interacting with its companion IC 5283, $1.3'$ to the NNE. It should be noted that various distances quoted in the literature are about twice the distance assumed in this paper. High-resolution VLA radio maps have been presented by e.g. Ulvestad et al. (1981); Condon et al. (1982, 1990) and Wilson et al. (1991). The radio emission (total flux density $S_{1.5GHz} = 160$ mJy) extends over the central $\approx 8''$ (1150 pc) and arises mostly from a circumnuclear starburst ‘ring’ (Wilson et al. 1986, 1991) surrounding a compact nuclear radio source (flux density $S_{4.9GHz} = 21$ mJy). The nucleus is a variable X-ray source (Barr, 1986; Fabbiano et al. 1992). The circumnuclear starburst dominates the energy budget as it represents two thirds of the bolometric luminosity of the entire galaxy (Genzel et al 1995) and is on the order of $10^{11} L_{\odot}$. The galaxy is a powerful object at infrared wavelengths and was mapped with millimeter arrays in the $J=1-0$ ^{12}CO line by Sanders et al. (1988, OVRO, $6''$) and Meixner et al. (1990, Hat Creek, $2''$), as well as more recently in the $J=2-1$ ^{12}CO and $J=1-0$ HCN lines by Davies et al. (2004, PdB, $0.7''$ and $2''$ respectively). Significant detail is, however, only revealed by the very high-resolution $J=2-1$ ^{12}CO map.

3. Observations and results

3.1. Observations

The observations described in this paper were carried out with the 15m James Clerk Maxwell Telescope (JCMT) on Mauna Kea (Hawaii) ¹ and with the IRAM 30m telescope on Pico Veleta (Spain). ²

3.1.1. JCMT Observations

At the epoch of the mapping observations (1991-2001) the absolute pointing of the telescope was good to about $3''$ r.m.s. as provided by pointing observations with the JCMT submillimeter bolometer. The spectra were calibrated in units of antenna temperature T_A^* , correcting for sideband gains, atmospheric emission in both sidebands and telescope efficiency. Calibration was regularly checked by observation of a standard line source. Further observational details are given in Tables 2 and 3. Most of the observations were carried out with the now defunct receivers A2, B3i and C2. Observations in 2001 were obtained with the current receivers B3 (330/345 GHz) and W/C (461 GHz). Full details on these receivers can be found at the JCMT website (<http://docs.jach.hawaii.edu/JCMT/HET/GUIDE/>). Up to 1993, we used a 2048-channel AOS backend covering a band of 500 MHz (650 km s^{-1} at 230 GHz). After that year, the DAS digital autocorrelator system was used in bands of 500 and 750 MHz. Integration times (on+off) given in Tables 2 are typical values appropriate to the maps. We subtracted second order baselines from the profiles. All spectra were scaled to a main-beam brightness temperature, $T_{mb} = T_A^*/\eta_{mb}$; values for the values of η_{mb} used are given in Tables 2 & 3.

All maps were made in rectangular grids (parameters given in Table 2), rotated to parallel the major axis of the galaxy mapped. The maps shown in this paper all have been rotated back to a regular grid in right ascension and declination. Some additional remarks are in order. In the case of NGC 1068, we combined our data as listed in Table 2 with those obtained by Papadopoulos & Seaquist (1999), taken from the JCMT archives, and re-reduced. The CO maps presented in this paper are based on both datasets. The velocity widths of the lines from the edge-on galaxy NGC 3079 were similar to the bandwidth of the JCMT backends used. For this reason, we observed the lines at three slightly different velocity settings. The resulting spectra were combined and concatenated to yield the final spectra.

3.1.2. IRAM observations

Observations of both ^{12}CO and ^{13}CO in the $J=1-0$ and $J=2-1$ transitions at resolutions of $21''$ and $12''$ respectively were obtained towards the centers of all galaxies with the IRAM 30m telescope in the period 2005-2007. We used the IRAM facility low-noise receivers A and B in both the 3mm and the 1mm bands. For backends we used the 1MHz

¹ The James Clerk Maxwell Telescope is operated on a joint basis between the United Kingdom Particle Physics and Astrophysics Council (PPARC), the Netherlands Organisation for Scientific Research (NWO) and the National Research Council of Canada (NRC).

² The IRAM 30m telescope is supported by INSU/CNRS (France), MPG (Germany), and IGN (Spain).

Table 4. Measured central ^{12}CO and ^{13}CO line intensities

	Beam Size ^a (")	NGC 1068		NGC 2146		NGC 3079		NGC 4826		NGC 7469	
		T_{mb} (mK)	$\int T_{\text{mb}}dV$ (K kms ⁻¹)	T_{mb} (mK)	$\int T_{\text{mb}}dV$ (K kms ⁻¹)	T_{mb} (mK)	$\int T_{\text{mb}}dV$ (K kms ⁻¹)	T_{mb} (mK)	$\int T_{\text{mb}}dV$ (K kms ⁻¹)	T_{mb} (mK)	$\int T_{\text{mb}}dV$ (K kms ⁻¹)
^{12}CO											
$J=1-0$	21	645	177±21	770	196±20	608	235±28	405	96±10 ^b	243	54±7
$J=2-1$	12	1080	266±32	1125	224±22	1085	454±54	425	82±8 ^b	545	124±15
	21	690	220±26	580	188±20	516	169±20	540	112±11	203	50±6
	<i>43</i>	—	99±12	—	74±7	—	94±11	—	53±5	—	17±2
$J=3-2$	14	630	166±20	1187	252±26	640	236±29	365	100±10	197	93±12
	<i>21</i>	—	114±14	—	153±17	—	138±17	—	63±6	—	45±6
$J=4-3$	11	1060	290±35	980	141±15	700	254±30	700	146±15	280	94±12
	<i>14</i>	—	231±28	—	122±13	—	218±26	—	139±14	—	69±8
	<i>21</i>	—	150±18	—	99±10	—	144±17	—	83±8	—	—
^{13}CO											
$J=1-0$	21	51	15.2±1.8	45	12.9±1.3	36	14.7±1.8	43	11.7±1.2 ^a	15	3.3±0.4
$J=2-1$	12	56	15.0±1.8	104	19.0±2.1	82	29.3±3.6	62	13.2±1.6 ^a	33	5.7±0.9
	21	46	17.1±2.0	106	16.8±1.8	26	10.8±1.3	65	14.9±1.7	25	4.2±0.7
$J=3-2$	14	43	10.7±1.3	86	18.3±1.9	60	26.0±3.1	42	9.3±1.1	25	3.5±0.7

Notes: ^a beams not directly observed but obtained from convolved maps (see Section 3.2) are in italics; ^b measured position is 10'' off nucleus.

and 4MHz filter banks, as well as the VESPA correlator. Initially, all four transitions were observed simultaneously, therefore with identical pointings. After this, the signal-to-noise ratio of the ^{13}CO profiles was increased by additional simultaneous observation of the two transitions, where we took care to ensure that the pointing was the same as for the earlier observations. Calibration and reduction procedures were standard and similar to those described in the previous section. The assumed η_{mb} values are likewise given in Tables 2 and 3. The IRAM observations were especially important not only because they provide measurements of the 3mm $J=1-0$ transitions not possible with the JCMT. The IRAM aperture is twice that of the JCMT, so that the combination of the two datasets provides $J=2-1/J=1-0$ and $J=3-2/J=2-1$ ratios in closely-matched beams,

3.2. Results

Central line profiles in all observed transitions are shown in Figs. 1 through 5. We mapped the distribution of the molecular gas in the galaxy centers in the $J=2-1$, $J=3-2$, and $J=4-3$ transitions, typically over an area of about one arcminute across. These maps are also shown in the Figures, as are the major axis position velocity diagrams of the central CO emission.

Measured line intensities towards the center of each galaxy are listed in Table 4. This Table contains entries both at full resolution, and at resolutions corresponding to those of transitions observed in larger beams. These entries were extracted from maps convolved to the resolution quoted. The convolution was carried out with the map interpolation function of the SPECX data reduction package³. This function interpolates, where necessary, the map intensities by using adjacent pixels out to a preset distance (usually 2 beams) and convolves the observed and interpolated data points with a two-dimensional Gaussian function ('beam') of predetermined halfwidth. This halfwidth is chosen such

that the actual observing beam convolved with the 2D-Gaussian would yield a beam corresponding to the desired resolution. Velocities in a position-velocity map can also be 'smoothed' by applying a convolving Gaussian function in a similar manner.

Finally, we have determined the line intensity ratios of the observed transitions at the center of the galaxies observed. These line ratios have been corrected for small offsets between the various datasets. They have been determined independently from the intensities given in Table 4. Specifically: (a) we used data taken at the same observing run wherever possible, (b) we determined ratios at various resolutions convolving the maps to the relevant beam widths, (c) we verified ratios by comparing profile shapes in addition to integrated intensities, and (d) the line ratios have been corrected for small offsets between the various datasets. In Table 5, whenever data were insufficient for convolution, or altogether lacking (e.g. [CI]), no entry is provided.

4. Analysis

4.1. Radiative transfer modeling of CO

We have modeled the observed ^{12}CO and ^{13}CO line intensities and ratios with the large velocity gradient (LVG) radiative transfer models described by Jansen (1995) and Jansen et al. (1994) – but see also Hogerheijde & van der Tak (2000) and the web page <http://www.strw.leidenuniv.nl/~michi/ratran/>. These codes provide model line intensities as a function of three input parameters per molecular gas component: gas kinetic temperature T_k , molecular hydrogen density $n(\text{H}_2)$ and the CO column density per unit velocity $N(\text{CO})/dV$. By comparing model to observed line *ratios*, we may identify the physical parameters best describing the actual conditions at the observed positions. Beam-averaged properties are determined by comparing observed and model intensities. In principle, with seven measured line intensities of two

³ <http://docs.jach.hawaii.edu/JCMT/cs/005/11/html/node129.html>

Table 5. Adopted velocity-integrated line ratios in galaxy centers

Transitions	Beam (")	NGC 1068	NGC 2146	NGC 3079	NGC 4826	NGC 7469
¹² CO						
(1-0)/(2-1)	21	0.97±0.18	1.04±0.17	1.39±0.27	1.02±0.17	1.08±0.16
(2-1)/(2-1)	12/21	1.21±0.24	1.19±0.17	2.69±0.54	1.08±0.22	2.47±0.38
(3-2)/(2-1)	21	0.52±0.11	0.82±0.12	0.72±0.14	0.60±0.09	0.86±0.13
(3-2)/(2-1)	12	0.71±0.14	0.99±0.15	0.61±0.12	0.84±0.18	0.87±0.13
(4-3)/(2-1)	21	0.68±0.13	0.65±0.16	0.76±0.15	0.74±0.12	—
(4-3)/(2-1)	12	1.00±0.20	0.63±0.11	0.56±0.11	—	0.66±0.11
¹² CO/ ¹³ CO						
(1-0)	21	11.9±1.8	15.2±2.0	16.2±2.4	8.2±1.2	16.2±2.4
(2-1)	21	11.4±1.7	11.2±1.7	13.5±2.0	7.2±1.2	16.4±1.7
(2-1)	12	15.8±2.4	11.8±1.5	15.2±2.2	6.2±0.9	20.5±3.0
(3-2)	14	15.3±2.2	13.3±2.0	9.1±1.4	10.8±2.6	15.3±2.3
(3-2)	21	13.3±2.0	—	—	—	—
[CI]/CO(2-1))	21	0.33±0.07	—	0.57±0.11	0.58±0.23	—

Table 6. Radiative transfer model parameters

No.	Component 1			Component 2			Ratio Comp. 1:2	¹² CO $\frac{(1-0)}{(2-1)}$	¹² CO $\frac{(3-2)}{(2-1)}$	Model Ratios ¹² CO/ ¹³ CO			
	Kin. Temp. T_k (K)	Gas Dens. $n(\text{H}_2)$ (cm^{-3})	Gradient $\frac{N(\text{CO})}{dV}$ ($\frac{\text{cm}^{-2}}{\text{km s}^{-1}}$)	Kin. Temp. T_k (K)	Gas Dens. $n(\text{H}_2)$ (cm^{-3})	Gradient $N(\text{CO})/dV$ ($\frac{\text{cm}^{-2}}{\text{km s}^{-1}}$)				$\frac{(4-3)}{(2-1)}$	(1-0)	(2-1)	(3-2)
NGC 1068													
1	60	1000	3.0×10^{17}	30	3000	0.06×10^{17}	1:9	1.08	0.62	0.32	10.9	10.9	13.2
2	30	3000	1.0×10^{17}	30	3000	0.06×10^{17}	1:4	0.99	0.62	0.28	13.2	10.6	12.2
NGC 2146													
3	125	1000	1.0×10^{17}	30	100000	0.3×10^{17}	11:9	1.09	0.86	0.64	15.5	11.3	13.3
4	150	1000	1.0×10^{17}	125	30000	1.0×10^{17}	6:1	1.06	0.83	0.60	15.3	11.5	13.3
NGC 3079													
5	150	100	0.3×10^{17}	30	100000	0.6×10^{17}	6:1	1.28	0.69	0.51	16.3	13.3	9.8
6	150	1000	1.0×10^{17}	20	10000	0.3×10^{17}	1:4	1.14	0.72	0.40	16.5	14.2	10.2
NGC 4826													
7	60	3000	1.0×10^{17}	10	1000	1.0×10^{17}	1:2	1.19	0.70	0.43	8.0	7.6	10.3
NGC 7469													
8	60	100000	0.6×10^{17}	30	500	0.3×10^{17}	1:6	1.06	0.80	0.65	15.8	18.5	16.4
9	30	100000	0.3×10^{17}	10	100	0.6×10^{17}	1:6	1.09	0.79	0.66	17.2	18.1	13.9

isotopes, properties of a single gas component are overdetermined as only five independent observables are required. In practice, this is mitigated by degeneracies such as occur for ¹²CO. In any case, we find that fits based on a single-component gas are almost always incapable of fully matching the data. However, we usually obtain good fits based on *two* gas components. The solutions for a two-component gas are slightly underdetermined but we can successfully compensate for this by introducing additional constraints as described below. The physical gas almost certainly has a much wider range of temperatures and densities. However, with the present data two components is the maximum that can be considered, as adding even one more component increases the number of free parameters to the point where solutions are physically meaningless. Thus, our two-component model gas is only an approximation of reality but it is decidedly superior to one-component model

solutions. As long as significant fractions of the total molecular gas mass are limited to similar segments of parameter space, they also provide a reasonably realistic model for the actual state of affairs. Specifically, our analysis is less sensitive to the occurrence of gas at very high densities and temperatures, but such gas is unlikely to contribute significantly to the total mass.

In order to reduce the number of free parameters, we assumed identical CO isotopical abundances for both gas components. Furthermore, in a small number of starburst galaxy centers (NGC 253, NGC 4945, M 82, IC 342, He 2-10), values of 40 ± 10 have been suggested for the isotopical abundance [¹²CO]/[¹³CO] (Mauersberger & Henkel 1993; Henkel et al. 1993, 1994, 1998; Bayet et al. 2004), somewhat higher than the characteristic value of 20–25 for the Milky Way nuclear region (Wilson & Rood 1994). We therefore have adopted an abundance value of [¹²CO]/[¹³CO] =

Table 7. Beam-averaged model parameters

Galaxy	No.	Beam-Averaged Column Densities			Outer Radius R (kpc)	Central H_2 Mass M_{H_2} ($10^8 M_\odot$)	Face-on Mass Density $\sigma(H_2)$ (M_\odot/pc^{-2})	Relative Mass Components 1:2
		$N(CO)$ ($10^{18} cm^{-2}$)	$N(C)$ ($10^{21} cm^{-2}$)	$N(H_2)$ ($10^{21} cm^{-2}$)				
NGC 1068	1/2	0.60	0.25	1.6	1.0	1.2	21	0.20:0.80
NGC 2146	3	0.50	0.40	1.6	1.5	1.4	18	0.75:0.25
	4	0.70	0.55	2.3	1.5	2.0	26	0.80:0.20
NGC 3079	5	1.20	0.50	3.0	0.9	1.8	19	0.80:0.20
	6	1.50	0.50	3.6	0.9	2.1	22	0.40:0.60
NGC 4826	7	0.85	0.45	2.4	0.3	0.3	23	0.30:0.70
NGC 7469	8/9	0.20	0.45	1.2	1.2	2.5	15	0.10:0.90

40 in our models. We identified acceptable fits by searching a grid of model parameter combinations ($10 K \leq T_k \leq 150 K$, $10^2 cm^{-3} \leq n(H_2) \leq 10^5 cm^{-3}$, $6 \times 10^{15} cm^{-2} \leq N(CO)/dV \leq 3 \times 10^{18} cm^{-2}$) for model line ratios matching the observed set, with the relative contribution of the two components as a free parameter. Solutions obtained in this way are not unique, but rather define a limited range of values in distinct regions of parameter space. For instance, variations in input parameters may to some extent compensate one another, producing identical line ratios for somewhat different combinations of input parameters. Among all possible solution sets, we have rejected those in which the denser gas component is also much hotter than the more tenuous component, because we consider the large pressure imbalances implied by such solutions physically implausible, certainly on the kiloparsec scales observed.

The results of our model fitting procedure are summarized in Table 6.

4.2. Beam-averaged molecular gas properties

The chemical models presented by van Dishoeck & Black (1988) show a strong dependence of the $N(C)/N(CO)$ column density ratio on the total carbon ($C+CO$) and molecular hydrogen column densities. If line intensities of all three species, CO, [CI] and [CII] are known, minimal assumptions suffice to deduce total carbon and hydrogen column densities and masses.

If C° and C^+ have not been observed, we can still relate the radiative transfer model results to molecular hydrogen column densities by taking the $[C]/[H]$ gas-phase abundance ratio as an additional constraint. We must then find the molecular hydrogen column density that satisfies both the total carbon $N_C = N(C) + N(CO)$ column-density and the carbon ratio $f_C = N(C)/N(CO)$ commensurate with the above-mentioned models and $[C]/[H]$ abundance. We intend to compare the results for various galaxies, several of which are lacking either [CI] or [CII] measurements, or both. Thus, for the sake of consistency, we use this second method for all galaxies, whether or not [CI] or [CII] have been detected.

Oxygen abundances and gradients of many nearby galaxies have been compiled by Vila-Costas & Edmunds (1992), Zaritsky et al. (1994), and Pilyugin, Vílchez & Contini (2004). Extrapolated to zero radius, the first two compilations imply nuclear metallicities many times solar. However, Pilyugin et al.'s more recent compilation yields nuclear metallicities on average only 1.5 times solar. These

are nevertheless quite uncertain, because the galaxy disk values and gradients were derived from HII regions at various distances to the center, and it is not very clear whether such results can be extrapolated to the rather different galactic center conditions. Another practical complication is that of our sample, only NGC 1068 is included in these compilations, although we have an estimate for NGC 7469 from X-ray observations (Blustin et al. 2007). In the following, we have conservatively assumed a metallicity twice solar to apply to the galaxy central regions. The results published by Garnett et al. (1999) suggest very similar carbon and oxygen abundances at these metallicities, so that we adopt $[C]/[H] \approx 1.0 \times 10^{-3}$. As a significant fraction of carbon is tied up in dust particles and thus unavailable in the gas-phase, we have also adopted a fractional correction factor $\delta_c = 0.27$ (see for instance van Dishoeck & Black 1988), so that $N_H/N_C = [2N(H_2) + N(HI)]/[N(CO) + N(CII) + N(CI)] = 3700$, uncertain by about a factor of two. In Table 7 we present beam-averaged column densities for CO and C ($=C^\circ + C^+$), as well as H_2 derived under the assumptions just discussed. As the observed peak CO intensities are significantly below the model peak intensities, only a small fraction of the (large) beam surface area can be filled with emitting material.

Although the analysis in terms of two gas components is superior to that assuming a single component, it is still not fully realistic. For instance, the assumption of e.g. *identical beam filling factors* for the various species (^{12}CO , ^{13}CO , C° , and C^+) is not a priori plausible. Fortunately, these assumptions are useful but not critical in the determination of beam-averaged parameters. If, by way of example, we assume a smaller beam filling factor, the model cloud intensity increases. This generally implies a higher model column-density which, however, is more strongly diluted by the beam. The beam-averaged column-density is modified only by the degree of non-linearity in the response of the model parameters to a change in filling factor, *not* by the magnitude of that change. A similar state of affairs exists with respect to *model degeneracy*, i.e different model parameter combinations yielding (almost) identical line ratios. Although, for instance, the model fractions of hot or dense gas may differ, the final derived *beam-averaged* molecular hydrogen densities are practically the same. In fact, the assumed gas-phase carbon abundance dominates the results. The derived beam-averaged column-densities (and projected mass densities) roughly scale inversely proportional to the square root of the abundance assumed: $N_{av} \propto [C]/[H]_{gas}^{-0.5}$. As our estimate of the central ele-

mental carbon abundance, and our estimate of the carbon depletion factor are unlikely to be wrong by more than a factor of two, the resulting uncertainty in the final values listed in Table 7 should be no more than 50%.

5. Discussion

5.1. NGC 1068

The *extended inner star-forming zone* has line ratios that do not allow for much variation of the gas properties. Given the size (deconvolved dimensions of $27 \times 24''$) of the region, its general appearance, and the relatively slight contribution of the compact circumnuclear disk, the emission in the lower CO transitions refers to the extended emission associated with the star-forming spiral arms and disk (see, for instance, Wynn-Williams, Becklin & Scoville 1985 or Le Floch et al. 2001). The major axis-velocity map shown in in Fig. 1 illustrates the dominance of the spiral arms in the $J=3-2$ ^{12}CO distribution in the shape of the bright maxima at the extreme velocities, with much less bright CO emission closer to the nucleus. The central minimum is not pronounced, however, because it is filled in by emission from the unresolved circumnuclear source (see also Fig. 6 in Helfer & Blitz 1995). We did not use the $J=4-3$ results in our analysis. The models predict a $J=4-3/J=2-1$ line ratio of about 0.3, only half of that actually observed (Table 3.2). However, much of the emission in this transition arises in the compact circumnuclear gas, rather than in the extended source (see Fig. 6). We find a relatively cool molecular gas ($T_{\text{kin}} \approx 30$ K) with densities ranging over ($n_{\text{H}_2} = 10^3\text{-}10^4 \text{ cm}^{-3}$). The inner star-forming zone shows up quite clearly in the high-resolution HI map by Brinks et al. (1997), reaching peak column densities $N(\text{HI}) \approx 3 \times 10^{21} \text{ cm}^{-2}$ in $8''$ beams. Such H_2 and HI values are typical values for photon-dominated regions (PDRs) associated with star formation.

Most, but not all (60%) carbon must be locked up in CO. The overall filling factor of the molecular gas is 7%. The molecular gas mass mapped over the central $2R = 2$ kpc is slightly more than $M_{\text{H}_2} = 10^8 M_{\odot}$, i.e a bit less than one per cent of the dynamical mass $M \approx 1.5 \times 10^{10}$ implied by the major-axis-velocity map in Fig 1.

The *compact circumnuclear gas* is reasonably well resolved by the $10''\text{-}14''$ beam data, but the lack of ^{13}CO intensities severely hamper attempts to model it. The ratio $^{12}\text{CO}/^{13}\text{CO} > 6$ implied by the BIMA observations by Helfer & Blitz (1995) does not present a significant constraint. Nevertheless, the models do imply that a significant fraction (10-50%) of this circumnuclear gas must have a density $n_{\text{H}_2} \approx 10^5 \text{ cm}^{-3}$ and a temperature of 30-60 K. This is consistent with the values estimated by Jackson et al. (1993), Tacconi et al. (1994), Helfer & Blitz (1995), Papadopoulos & Seaquist (1999), and Usero et al. (2004). The remainder of the gas must be rather tenuous ($n_{\text{H}_2} = 100 - 1000 \text{ cm}^{-3}$) at an undetermined temperature. The emission from this gas is particularly prominent in the $J=4-3$ ^{12}CO and [CI] maps shown in Fig. 6, and the maps by Jackson et al. (1993) and Helfer & Blitz (1995) show a similar prominent role for $J=1-0$ HCN. The lack of ^{13}CO emission precisely at the nucleus where the [CI] emission is strongest, implies that the actual [CI]/ ^{13}CO (2-1) ratio is significantly higher than the beam-confused value given by Israel & Baas (2002) – already one of the highest

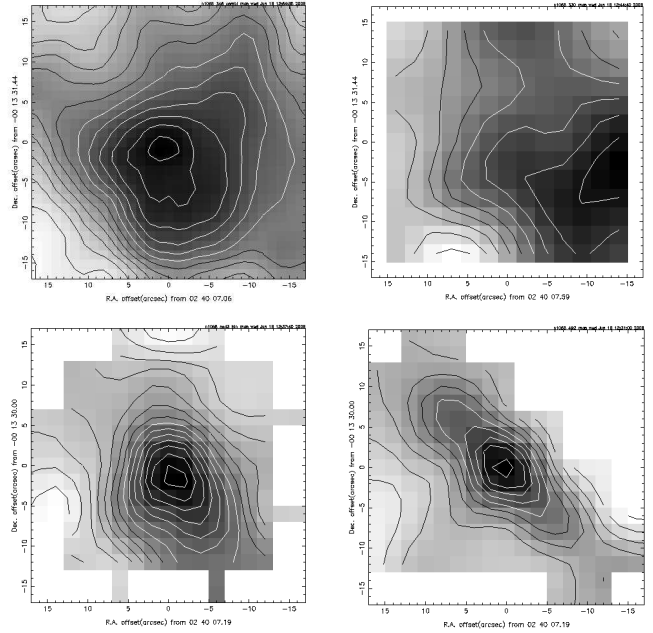


Fig. 6. Central $30''$ of NGC 1068. Top left $J = 3 - 2$ ^{12}CO with contour step of 10 K km s^{-1} , top right $J = 3 - 2$ ^{13}CO with contour step of 1 K km s^{-1} , bottom left $J = 4 - 3$ ^{12}CO with contour step of 20 K km s^{-1} , bottom right [CI] with contour step of 10 K km s^{-1} . Note dominance of the unresolved nuclear source in the latter two maps

in their galaxy sample. Inside the star-forming spiral arms, and thus also towards the nucleus, there is very little HI ($N(\text{HI}) \leq 2 \times 10^{20} \text{ cm}^{-2}$ cf Brinks et al. 1997). Much of the circumnuclear gas thus is dense and warm, and appears to be excited by the AGN rather than by luminous stars (cf Lepp & Dalgarno 1996; Usero et al. 2004, Meijerink et al. 2006, 2007). Strong neutral carbon emission is characteristic for X-ray excitation (Meijerink et al. 2007).

The *extended bar*. Particularly interesting is the structure exhibited by [CI]. The unresolved intense source, coinciding with the nucleus, is accompanied by tongues of [CI] emission stretching out to the northeast and southwest in a position angle of about 45° . The two extensions are real, and not due to instrumental effects, as the [CI] profiles in the map accurately represent the rapidly changing velocity field. This extended [CI] emission is in the same position angle as the northeastern radio jet (Wilson & Ulvestad 1987), and coincides with the northeastern near-infrared [FeII] line and X-ray continuum emission extensions (Bletz et al. 1994; Young et al. 2001). However, the carbon emission in our map also extends in the *opposite* direction and thus more closely corresponds to the distribution of the near-infrared K-band continuum emission (Rotaciuc et al. 1991; Davies, Sugai & Ward 1998), the near-infrared *polarized* emission (Lumsden et al. 1999), and the $J=1-0$ ^{12}CO emission in the fully-UV-sampled array map by Helfer & Blitz (1995). Interestingly, the southwestern molecular gas extension clearly seen in their map is absent in the ^{12}CO maps by Schinnerer et al. (2000) and Usero et al. (2004) that lack the short-spacing information. There is no HI emission corresponding to the [CI] emission (cf Brinks et al. 1997), although some HI *absorption* ($N(\text{HI}) = 1 - 2 \times 10^{21} \text{ cm}^{-2}$ in a $\approx 2''$ beam) is seen against the continuum of the southwestern bar. The nature of the extended carbon emission is

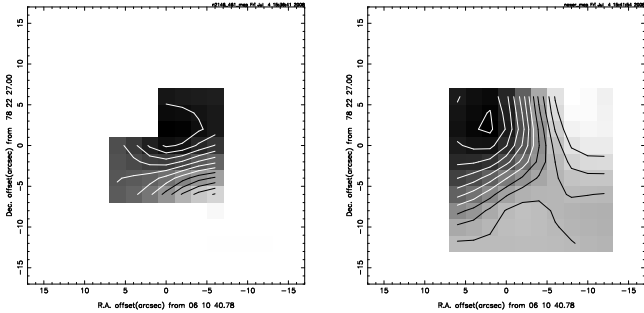


Fig. 7. Central 30'' of NGC 2146. On the left $J=4-3$ ^{12}CO , and on the right $J=6-5$ ^{12}CO . Both maps have contour steps of 10 K km s^{-1} . The relatively high intensity of $J=6-5$ ^{12}CO confirms that much of the molecular gas in NGC 2146 is at elevated temperatures.

not clear. Its presence at directions devoid of X-ray or [FeII] emission suggests that the observed strong [CI] emission does not originate in an X-ray-excited dense gas. Rather it appears that this emission arises from (photo)dissociated gas streaming along the stellar and molecular bar discussed by Tacconi et al. (1994) and Helfer & Blitz (1995). Its nature would thus be different from that of the neutral carbon in the circumnuclear source.

5.2. NGC 2146

Our maps show bright CO extending over $37''$ ($J=3-2$ size) coincident with the bright central starburst region. The deconvolved extent of $28''$ (2.4 kpc) is identical to that found by Dumke et al. (2001) with a larger beam, and indeed to the extent of the resolved ^{12}CO and dust emission observed at much higher resolution with the various millimeter arrays (Young et al. 1988b; Jackson & Ho 1988; Greve et al. 2006). Thus, there appears to be very little molecular gas beyond radii of a kiloparsec. The CO extent also corresponds quite closely to that of the bright radio emission in the VLA maps by Kronberg & Biermann (1981) and Zhao et al. (1996); the array of discrete radio sources mapped at very high resolution ($0.4''$) by Tarchi et al. (2000) covers a full span of $25''$. The appearance of the high-resolution CO maps, the unmistakable double structure in maps of peak rather than integrated brightness temperature (not shown) and the shape of the CO distribution in the major axis-velocity diagram (Fig. 2), exhibiting minimum intensity at the galaxy center, establish that the observed CO does not homogeneously fill the central volume. Rather, it must be distributed in a warped ring (Greve et al. 2006), or much more likely, in CO-enhanced spiral arms seen mostly edge-on. The central few hundred parsec should be largely free of gas. The ionized gas measured by Zhao et al. (1996) appears to cover the full range of velocities seen in Fig. 2 within the central $5''$. Tarchi et al. (2002) found two water kilomasers marking star-forming regions. One is located in the northwestern CO emitting region, 7 from the center with $V_{LSR} \approx 825 \text{ km s}^{-1}$, and the other projected very close to the nucleus with $V_{LSR} = 1010 \text{ km s}^{-1}$, also within the CO contours in Fig 2-bottom.

Our LVG analysis effectively yields two different model solutions (see Table 6). The first one combines quite warm ($T_{kin} = 125 \text{ K}$) and not very dense ($n_{\text{H}_2} = 10^3 \text{ cm}^{-3}$) molecular gas with a three times smaller amount of cooler

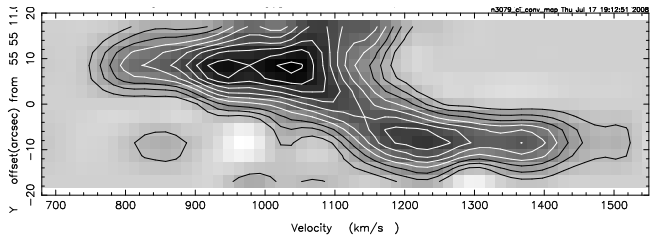


Fig. 8. Major-axis-velocity map of the [CI] emission from NGC 3079. Contour step is 40 mK. Note relative minimum of [CI] emission in the center of NGC 3079.

($T_{kin} = 30 \text{ K}$), much denser ($n_{\text{H}_2} = 10^5 \text{ cm}^{-3}$) gas. The second solution finds essentially all molecular gas to be warm ($T_{kin} = 150 \text{ K}$), but most of it is not very dense ($n_{\text{H}_2} = 10^3 \text{ cm}^{-3}$) with a small fraction reaching densities more than an order of magnitude higher ($n_{\text{H}_2} = 3 \times 10^4 \text{ cm}^{-3}$).

However, we have also detected $J=6-5$ ^{12}CO emission from the center of NGC 2146, at intensities of about 0.5 to 0.7 times that of the $J=4-3$ ^{12}CO emission in the same beam (Figure 7). The second of the two model solutions ('all gas is warm') is in much better agreement with this ratio than the first. In terms of overall results, As Table 7 shows, the difference is not great in terms of beam-averaged results, as indeed should be expected from the discussion in Section 4.

5.3. NGC 3079

Our ^{12}CO maps (see Fig. 3) show a just-resolved CO core superposed on the more extended emission of the edge-on galaxy. In Fig 3-bottom the rapidly rotating gas clearly stands out from the more sedately moving gas in the disk of NGC 3079. The central velocity field is complex. The dynamics of the central molecular gas of NGC 3079 have been discussed in considerable detail by Sofue et al. (2001) and Koda et al. (2002) who propose the presence of both a weak bar, and an extremely massive black hole in the center. The diameter of the molecular core in the galaxy plane is consistent with the diameter of $14''$ derived from millimeter array maps (e.g. Sofue et al. 2001). In the $J=4-3$ ^{12}CO line, the core appears to be more compact than in the lower transitions, but this just reflects the contribution from the large-scale disk weakening with increasing transition.

The behavior of the neutral carbon emission differs from that in NGC 1068 described above. In NGC 3079, the [CI] emission does not peak at the center of the galaxy. Rather, as Fig. 8 shows, it peaks at either side of the galaxy, and the emission from the center is relatively weak. This suggests a distribution in which a larger fraction of the central region is free of neutral carbon than of carbon monoxide. As was the case for NGC 2146, the observed line ratios allow two essentially different LVG model solutions. The first one provides a rather good fit to the data and puts a very large fraction of the molecular gas in a hot ($T_{kin} = 150 \text{ K}$), tenuous ($n_{\text{H}_2} = 10^2 \text{ cm}^{-3}$) gas, leaving a relatively small fraction of the gas in a cool ($T_{kin} = 30 \text{ K}$) and very dense ($n_{\text{H}_2} = 10^5 \text{ cm}^{-3}$) molecular gas. The second solution provides a fit that is not as good, but still within the line ratio uncertainties. Now, slightly less than half of the molecular gas is hot ($T_{kin} = 150 \text{ K}$) and modestly

dense ($n_{\text{H}_2} = 10^3 \text{ cm}^{-3}$), whereas the remainder is cold ($T_{\text{kin}} = 20 \text{ K}$) and reasonably dense ($n_{\text{H}_2} = 10^4 \text{ cm}^{-3}$). Braine et al. (1997) found a mean dust temperature of 30 K, which suggests that the second model solution is more likely than the first. The mean molecular gas column densities of NGC 3079 are highest of all the sample galaxies, which is not surprising in view of the almost exactly edge-on orientation of the galaxy, and the high extinction ($A_V \geq 6^m$, Israel et al. 1998) towards the very center. The central molecular mass is $M_{\text{H}_2} \approx 2 \times 10^8 M_\odot$, for either model solution. This mass is much lower than the values derived by the various authors quoted above using ‘standard’ CO-to- H_2 conversion factors. It is, however, very close to the mass derived by Braine et al. (1997) using a different method. An important consequence of this lower molecular gas mass determination is that the gas no longer constitutes such a large fraction (half!) of the dynamical mass.

5.4. NGC 4826

The maps in Fig. 4 show that essentially all molecular gas is contained within a distance of $30''$ (600 pc) from the nucleus – i.e. all molecular gas is located within the radius at which the rotation curve reverses sign. This is particularly well illustrated by the $J=2-1$ ^{12}CO major-axis velocity map at bottom. Unlike the p-V maps of the other galaxies, this map shows very clear boundaries at either side. Although the velocity-integrated CO emission appears to be peaked on the center in all maps, the position-velocity maps in Figs. 4 and 9 show that this is not the case. In all transitions the CO emission reaches a minimum at the center. This is also seen in the higher-resolution array maps published by Casoli & Gerin (1993) and García-Burillo et al. (2003).

In Fig. 4, the $J=3-2$ ^{12}CO distribution appears more compact than that in the $J=2-1$ transition. This is partly an effect caused by the significantly higher resolution ($14''$ vs $21''$) of the former. However, closer analysis shows that the higher-excited CO gas is indeed more concentrated than the CO in the ground states. In all observed transitions, CO emission extends out to $R = 30''$ (see e.g. Fig. 9-top), but the half-width (FWHM) of the CO distribution, corrected for finite beam width, is $43''$ in the $J=2-1$ transition, and only $20''$ ($R = 200 \text{ pc}$) in both the $J=3-2$ and $J=4-3$ transitions (*cf* Fig. 9-bottom), as well as in [CI] (not shown). It thus appears that the hotter molecular gas is preferentially found closer to the starburst center.

The ^{12}CO and ^{13}CO line ratios observed in NGC 4826 are not very well fitted by the model parameters given in Table 6. In particular the $J=4-3$ ^{12}CO line is too strong, a situation we also found in the center of NGC 1068. The high temperature of this relatively dense ($n_{\text{H}_2} \approx 3000 \text{ cm}^{-3}$) gas close to the nucleus opens up the possibility that X-ray emission from the latter plays a role in the excitation. A minor radio source (Hummel et al. 1987; Turner & Ho 1994) in the center suggests the presence of a weak AGN (see also García-Burillo et al. 2003; Haan et al. 2008). It is noteworthy that the molecular gas constitution changes away from the central peak. For instance, at a position $18''$ (355 pc) ESE from the nucleus we find line ratios that suggest either a kinetic temperature of about 30 K and a density of about 3000 cm^{-3} , or comparable amounts of cold, very dense ($T_{\text{kin}} = 10 \text{ K}$, $n_{\text{H}_2} = 10^5 \text{ cm}^{-3}$) and warm, very tenuous ($T_{\text{kin}} = 60 \text{ K}$, $n_{\text{H}_2} = 10^2 \text{ cm}^{-3}$) molecular gas. The lack of more ^{13}CO measurements makes it impossi-

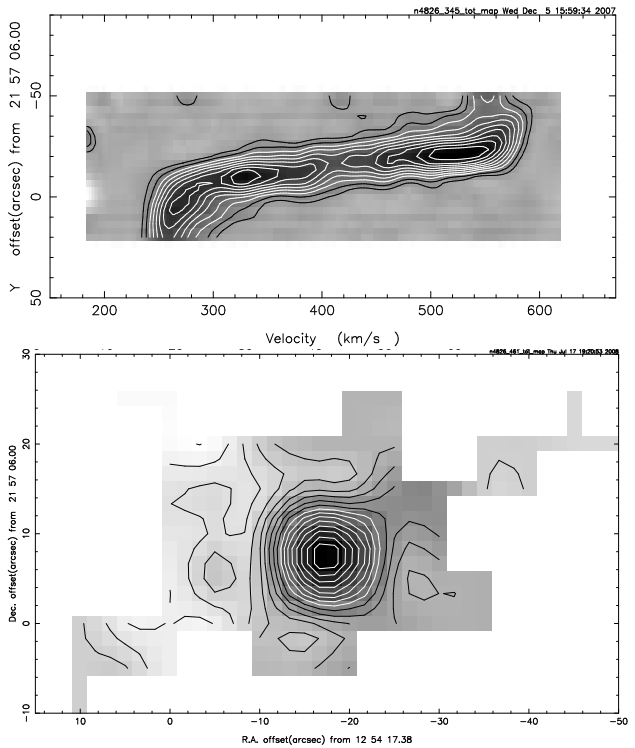


Fig. 9. Top: major-axis-velocity diagram of the $J=3-2$ ^{12}CO emission from NGC 4826. Contour step is 40 mK. Bottom: $J=4-3$ ^{12}CO map of NGC 4826 with contour step of 10 K km s^{-1} .

ble to choose between these alternatives, but especially the first one is compatible with molecular gas heated by UV radiation from luminous stars.

5.5. NGC 7469

As expected, our maps (Fig. 5) do not show much detail in this distant galaxy. Nevertheless, the $J=3-2$ ^{12}CO maps show emission from the center superposed on a more extended disk. Unfortunately, our $J=4-3$ ^{12}CO map is incomplete in the direction of the $J=3-2$ extension. Our angular resolution is insufficient to resolve the rotation curve of NGC 7469, but once again it can be clearly seen that the nucleus itself is at a relative CO minimum, as confirmed by the array maps obtained by Davies et al. (2004). We may thus expect the molecular gas parameters to be dominated by the extended starburst region rather than by the immediate surroundings of the AGN. The observed line ratios are well-fitted by the model parameters listed in Table 6. These imply that a small amount (typically a few times $10^7 M_\odot$) of the molecular gas is modestly warm ($T_{\text{kin}} = 30-60 \text{ K}$) and rather dense ($n_{\text{H}_2} = 10^5 \text{ cm}^{-3}$). It is tempting to associate this relatively small amount with the AGN-irradiated gas also seen in near-infrared H_2 emission (Genzel et al. 1995; Davies et al. 2004). The bulk of the molecular gas has mean temperatures ($T_{\text{kin}} = 1-30 \text{ K}$) and mean densities ($n_{\text{H}_2} = 10^2 - 10^3 \text{ cm}^{-3}$) appropriate to extended star formation in the disk and spiral arms.

5.6. Column densities and masses

Characteristically, we find H_2 column densities averaged over a $21''$ beam of roughly $1\text{--}3 \times 10^{21} \text{ cm}^{-2}$, corresponding to total hydrogen columns of $2\text{--}6 \times 10^{21} \text{ cm}^{-2}$. These total columns also include the ambient contribution by neutral atomic hydrogen which we have so far neglected. HI absorption column densities actually measured towards these galaxies often exceed the H_2 column densities listed in Table 7. Towards NGC 1068 HI column densities $N(\text{HI}) = (1\text{--}2) \times 10^{21} \text{ cm}^{-2}$ (Brinks et al. 1997) are seen, but towards NGC 2146 peaks are up to six times higher than our average H_2 value, and reach as high as $N(\text{HI}) = (5\text{--}12) \times 10^{21} \text{ cm}^{-2}$ (Tarchi et al. 2002) in a $2.1'' \times 1.5''$ beam. Towards the nucleus of the edge-on galaxy NGC 3079, Pedlar et al. (1996) even find $N(\text{HI}) = 27 \times 10^{21} \text{ cm}^{-2}$ in a $4'' \times 3''$ beam. Compared to this, the mostly face-on galaxy NGC 7469 has rather moderate neutral atomic hydrogen column densities $N(\text{HI}) \approx 3 \times 10^{21} \text{ cm}^{-2}$, seen directly in absorption against the nucleus (Beswick et al. 2002) and also implied by X-ray absorption (Barr, 1986). Especially in edge-on galaxies, not all HI seen in absorption necessarily resides in the central region we have sampled. Moreover, in all these cases the effective absorbing area is much smaller (by factors of 30 to 150) than the large $21''$ beam over which we have averaged our H_2 in Table 7. Our models imply CO, hence H_2 , surface filling factors of 5–8 for NGC 2146, NGC 4826, and NGC 7469, of 15 for NGC 1068, and 33 for NGC 3079. This suggests that the HI contribution to the total hydrogen column densities implied by the models is very small for NGC 1068 (on the order of a few per cent), and somewhat more (10–30 per cent) for NGC 2146, NGC 3079 and NGC 7469. In view of the uncertainty of a factor of two inherent in the model values, the error introduced by neglecting the HI contribution is negligible.

Our H_2 masses are much lower than those calculated previously by authors who used a ‘standard’ CO-to- H_2 conversion factor X . For instance, in the center of NGC 2146 we find a molecular hydrogen mass $M_{\text{H}_2} \approx 2 \times 10^8 M_\odot$, a factor of 23 lower than the mass listed by Greve et al. (2006). Even taking into account that these authors used the rather high conversion ($X = 3 \times 10^{20} \text{ cm}^{-2}/(\text{K kms}^{-1})$), there is still an order of magnitude difference with our result. In the galaxy centers discussed here, we find $X = 0.1\text{--}0.2 \times 10^{20} \text{ cm}^{-2}/(\text{K kms}^{-1})$ which is a factor of 10–20 lower than the ‘standard’ Milky Way X factors (see also Strong et al. 2004), but quite similar to those found in other galaxy centers (see Israel & Baas 2003 and references therein). Clearly, X factors derived for molecular clouds in the Solar Neighborhood do not apply to molecular gas in the very different environment posed by galaxy centers. We also note that the present results are consistent with the low values derived independently for the same galaxy centers by other authors from e.g. analysis of infrared observations (*cf* Genzel et al. 1995; Braine et al. 1997; Papadopoulos & Allen, 2000; Usero et al. 2004; Davies et al. 2004). Using the ‘standard’ value of X , authors in the past have concluded to very high gas mass fractions (up to half of the dynamical mass) in the centers of galaxies. With the revised low values, there is no longer a need to assume such extreme conditions. In fact, in our galaxies we find much more modest mass ratios $M_{\text{H}_2}/M_{\text{dyn}} \approx 0.5\text{--}1.0\%$.

5.7. Temperature and excitation

Although a classical UV-illuminated photon-dominated region (PDR) associated with a star-forming region may reach quite high kinetic temperatures, the amount of gas at such elevated temperatures is rather small and limited to the immediate vicinity of the stellar heating source. It is very difficult, even in intense star-forming regions, to reach globally averaged temperatures in excess of 20–30 K. An example will illustrate this. If the heating is provided by luminous ($L = 0.5\text{--}2.6 \times 10^6 L_\odot$, Vacca et al. 1996) O5 stars, and perfect temperature equilibrium is assumed, the separation between star and heated gas should be about 1.5–2.5 pc at 20 K, and only 0.6–1.0 pc at 30 K.

When we look at Table 6 we see that only the molecular line emission from the clear *Seyfert* galaxies NGC 1068 and NGC 7469 may arise from molecular gas dominated by a *starburst*. In the previous section, we have seen that in either galaxy our resolution was insufficient to separate the emission from the circumnuclear molecular gas from that of the much more extended molecular gas associated with the more *starburst*. We may therefore expect that observations similar to those presented in this paper, but conducted at substantially higher resolutions, might indeed require a different excitation for the gas close to the nucleus. As also noted above, there are already indications that this so in NGC 1068. In this respect, millimeter-array observations of this galaxy in high- J transitions of both ^{12}CO and ^{13}CO (SMA, ALMA) would be quite interesting.

Much if not all of the molecular gas in NGC 2146, which appears to be a *starburst-dominated* galaxy, is in fact far too hot ($T_{\text{kin}} = 125\text{--}150$ K) to be excited by UV photons from luminous stars. The situation is more ambiguous in the merger galaxy NGC 4826, where two thirds of the mass is probably heated in PDR fashion, but one third of the gas is again too hot with $T_{\text{kin}} \approx 60$ K. In NGC 3079, 20–60% of the gas may be heated by the *starburst* that is present at a few hundred parsec from the nucleus, but the remaining relatively diffuse gas is far too hot with a temperature as high as $T_{\text{kin}} \approx 150$ K. It is noteworthy that the two galaxies with the hottest gas (NGC 2146 and NGC 3079) are both associated with a wind-driven X-ray outflow (Armus et al. 1995; Della Ceca et al. 1999; Pietsch et al. 1998). One might speculate that the hot molecular gas component is efficiently heated by the X-rays from these flows (see Meijerink et al. 2006, 2007) rather than by the UV photons from the *starburst*.

6. Conclusions

1. We have observed the centers of five galaxies with significant central activity in the first four transitions of ^{12}CO and the first three transitions of ^{13}CO , and three of them also in the lower transition of [CI].
2. All galaxies were mapped over at least $1' \times 1'$ in the $J=2\text{--}1$ and $J=3\text{--}2$ and over smaller areas in the $J=4\text{--}3$ transitions of ^{12}CO .
3. The line ratios, reduced to a standard $21''$ beam vary significantly in the sample galaxies. In general, the $J=4\text{--}3$ line is still relatively strong, indicating elevated temperatures for the molecular gas.
4. Optical depths in ^{12}CO appear not to be very high, with $^{12}\text{CO}/^{13}\text{CO}$ ratios generally in the range of 11–16. Exceptions are NGC 4826 and NGC 7469. The first,

- a merger galaxy, has isotopic ratios in the range 6-8 suggesting somewhat higher optical depths reminiscent of extended molecular clouds in the Solar Neighborhood. On the other hand, the distant Seyfert galaxy NGC 7469 has isotopic ratios in the range of 16-20, suggesting that much of the gas in this galaxy has a low optical depth characteristic of relatively tenuous gas.
5. The molecular gas is present in the form of clearly identifiable central condensations of outer radius $R = 0.3 - 1.5$ kpc. In all galaxies, the molecular gas distribution exhibits a local minimum at the nucleus itself.
 6. In all galaxy central regions, we find moderate H_2 masses of $1 - 3 \times 10^8 M_\odot$, except in the nearby NGC 4826 where the mass is no more than $3 \times 10^7 M_\odot$. These masses are typically about one per cent of the dynamical mass in the same region. The CO-to- H_2 conversion factors X implied by these masses and the observed $J=1-0$ ^{12}CO line intensities is typically an order of magnitude lower than the 'standard' Solar Neighborhood X -factor.
 7. Intriguingly, the excitation of molecular gas in the Seyfert galaxies NGC 1068 and NGC 7469 appears to be dominated by UV-photons from the extended circumnuclear starburst. In contrast, the molecular gas in the starburst galaxy NGC 2146, and part of the molecular gas in NGC 3079 (starburst cum AGN) are probably excited by Xrays from their massive wind-driven outflows. The situation for NGC 4826 is less clear.

Acknowledgements. I am much indebted to the late Fred Baas, who died suddenly and far too early in 2001, for carefully planning and performing many of the observations described in this paper. I also thank the various JCMT observers who made additional observations in queue mode. Finally, it is always a pleasure to thank the personnel of both the JCMT and the IRAM 30m telescope for their able and generous support.

References

- Armus L., Shupe D.L., Matthews K., et al. 1994, in: 'Infrared Astronomy with Arrays', ed. I. McLean, Kluwer (Dordrecht), p. 501
- Armus L., Heckman T.M., Weaver K.A., & Lehnert M.D., 1995, ApJ 445, 666
- Bayet E., Gerin M., Phillips T.G., & Contursi A., 2004, A&A 427, 45
- Beswick R. J., Pedlar A., & McDonald A.R., 2002 MNRAS 335, 1091
- Blustin A.J., Kriss G.A., Holezer T., et al. 2007, A&A 466, 107
- Braun R., Walterbos R.A.M., Kennicutt R.C., & Tacconi L.J., 1994, ApJ 420, 558
- Braine J., Guélin M., Dumke M., et al. 1997, A&A 326, 963
- Braun R., Walterbos R.A.M., & Kennicutt R.C., 1992, Nature 360, 442
- Braun R., Oosterloo T.A., Morganti R., Klein U., & Beck R., 2007, A&A 461, 455
- Blietz M., Cameron S., Drapatz S., et al. 1994 ApJ 421, 92
- Brinks E., Skillman E. D., Terlevich R. J., & Terlevich E., 1997 Ap&SS248, 23
- Casoli F., & Gerin, 1993, A&A 279, L41
- Cecil G., Blad-Hawthorn J., Veilleux S., & Filippenko A.V., 2001 ApJ 555, 338
- Condon J.J., Condon M.A., Gisler G., & Puschell J.J., 1982, ApJ 252, 102
- Condon J.J., Helou G., Sanders D.B., & Soifer B.T., 1990 ApJS 73, 359
- Condon J.J., Helou G., Sanders D.B., & Soifer B.T., 1996 ApJS 103, 81
- Crawford M.K., Genzel R., Townes C.H. & Watson D.M., 1985 A&A 291, 755
- Davies R.I., Sugai H., & Ward M.J., 1998 MNRAS 295, 43
- Davies R.I., Tacconi L.J., & Genzel R., 2004 ApJ 602, 148
- de Bruyn A.G., 1977, A&A 58, 221
- Dumke M., Nieten Ch., Thuma G., Wielebinski R. & Walsh W., 2001 A&A 373, 853
- Della Ceca R., Griffiths R.E., Heckman T.M., Lehnert M.D., Weaver K.A., 1999, ApJ 514, 772
- Fabbiano G., Kim D.-W., & Trinchieri G., 1992 ApJS 80, 531
- Gallimore J.F., Baum S.A., O'Dea C.P., Brinks E., & Pedlar A., 1994, ApJL 422, L13
- García-Burillo S., Combes F., Hunt L.K., et al., 2003 A&A 407, 485
- Garnett D.R., Shields G.A., Peimbert M., et al. 1999 ApJ 513, 168
- Genzel R., Weitzel L., Tacconi-Garman E., et al. 1995, ApJ 444, 129
- Gerin M., & Phillips T.G., 2000, ApJ 537, 644
- Greve A., Neininger N., Sievers A., & Tarchi A., 2006, A&A 459, 441
- Haan S., Schinnerer E., Mundell C.G., García-Burillo S., & Combes F., 2008 AJ 135, 232
- Hawarden T.G., Israel F.P., Geballe T.R., & Wade R., 1995, MNRAS 376, 1197
- Helfer T.T., & Blitz L., 1995 ApJ 450, 90
- Helfer T.T., Thornley M.D., Regan M.W., et al. 2003, ApJS 145, 259
- Henkel C., Mauersberger R., Wiklind T., et al. 1993, A&A 268, L17
- Henkel C., Whiteoak J.B., & Mauersberger R., 1994 A&A 284, 17
- Henkel C., Chiu Y.-N., Mauersberger R. & Whiteoak J.B., 1998 A&A 329, 443
- Hummel E., van der Hulst J.M., Keel W.C., & Kennicutt R.C., 1987 A&AS 70, 517
- Hogerheijde M.R., & van der Tak F.F.S., 2000 A&A 362, 697
- Impellizzeri C.M.V., Henkel C., Roy, A.L., & Menten K.M., 2008, A&A 484, L43
- Inui T., Matsumoto H., Tsuru, T.G., Koyama K., Matsushita S., & Peck A.B., 2005 PASJ 57, 135
- Irwin J.A., & Saikia D.J., 2003, MNRAS 344, 977
- Israel F.P., White G.J., & Baas F., 1995, A&A 302, 343
- Israel F.P., van der Werf P.P., Hawarden T.G., & Aspin C., 1998 A&A 336, 433
- Israel F.P., & Baas F., 1999, A&A 351, 10
- Israel F.P., & Baas F., 2001, A&A 371, 433 (Paper I)
- Israel F.P., & Baas F., 2002, A&A 383, 82
- Israel F.P., & Baas F., 2003, A&A 404, 495 (Paper II)
- Israel F.P., Tilanus R.P.J., & Baas F., 2006, A&A 445, 907 (Paper III)
- Irwin J.A., & Seaquist E. R., 1991 ApJ 371, 111
- Irwin J.A., & Sofue Y., 19921 ApJL 396, L75
- Jackson J.M., & Ho P.T.P., 1988, ApJL 324, L5
- Jackson J.M., Paglione T.A.D., Ishizuki S., & Nquyen-Q-Rieu, 1993, ApJL 418, L13
- Jansen D.J., 1995, Ph.D. thesis, University of Leiden (NL)
- Jansen D.J., van Dishoeck E.F. & Black J.H., 1994, A&A , 282, 605
- Kaneko N., Morita K., Fukui Y., and 5 other authors, 1989, ApJ 337, 691
- Kaneko N., Morita K., Fukui Y., and 4 other authors, 1992, PASJ 44, 341
- Koda J., Sofue Y., Kohno K., et al., 2002, ApJ 573, 105
- Kronberg P.P., & Biermann, P., 1981, ApJ 243, 89
- Le Floc'h E., Mirabel L.F., Laurent O., et al. 2001 A&A 367, 487
- Lepp S., & Dalgarno A., 1996 A&A , 306, L21
- Lisenfeld U., Alexander P., Pooley G.G., & Wilding, T. 1996 MNRAS 281, 301
- Lumsden S.L., Moore, T.J.T., Smith C., et al. 1999 MNRAS 303, 209
- Mauersberger R. & Henkel C., 1993 Rev. Mod. Astron. 6, 69
- Meijerink R., Spaans M., & Israel F.P., 2006 ApJL 650, L103
- Meijerink R., Spaans M., & Israel F.P., 2007 A&A 461, 793
- Meixner M., Puchalsky R., Blitz L., Wright M., & Heckman T., 1990 ApJ 354, 158
- Moustakas J., & Kennicutt R.C., 2006 ApJ 651, 155
- Papadopoulos P.P., & Seaquist E.R., 1999, ApJ 516, 114
- Paglione T.A.D., Wall W. F., Young J.S. et al. 2001, ApJ 135, 183
- Pedlar A., Mundell C.G., Gallimore J.F., Baum S.A., & O'Dea C.P., 1996, VA, 40, 91
- Pietsch W., Trinchieri G., & Vogler A., 1998, A&A 340, 351
- Pilyugin L.S., Vílchez J.M., & Contini T., 2003 A&A 425, 849
- Planesas P., Gómez-González J., & Martín-Pintado J., 1989, A&A 216, 1
- Planesas P., Scoville N.Z., & Myers S.T., 1991, ApJ 369, 364
- Rix H.-W., Kennicutt R.C., Braun R., & Walterbos R.A.M., 1995, ApJ 438, 155
- Rosolowsky E., & Blitz L., 2005, ApJ 623, 826
- Rotaciuc V., Krabbe A., Cameron M., et al. 1991 ApJL 370, L23
- Rubin V.C., 1994, AJ 107, 173
- Sakamoto K., Okumura S.K., Ishizuki S. & Scoville N.Z., 1999 ApJS 124, 403

- Sandage A. & Bedke J., 1994, *The Carnegie Atlas of Galaxies*. Volume I, Carnegie Institution of Washington
- Schinnerer E., Eckart A., Tacconi L.J., Genzel R., & Downes D., 2000, *ApJ* 533, 850
- Scoville N.Z., Young J. S. & Lucy L.B., 1983, *ApJ* 270, 443
- Sil'chenko O.K., 1996, *AL* 22, 108
- Sofue Y., & Irwin J.A., 1992, *PASJ* 44, 353
- Sofue Y., Koda J., Kohno K., et al. 2001, *ApJL* 547, L115
- Sternberg A., Genzel R., & Tacconi L., 1994, *ApJL* 436, L131
- Stacey G.J., Geis N., Genzel R., et al. 1985 *A&A* 373, 423
- Strong A.W., Moskalenko I.V., Reimer O., Digel S., & Diehl R., 2004 *A&A* 422, 47
- Tacconi L.J., Genzel R., Blietz M., Cameron M., Harris A.I., & Madden S., 1994, *ApJL* 426, L77
- Tacconi L.J., Blietz M., Cameron M., et al., 1996, *VA* 40, 23
- Tarchi A., Neininger N., Greve A., et al. 2000, *A&A* 358, 95
- Tarchi A., Henkel C., Peck A.B., & Menten K.M., 2002, *A&A* 389, 39
- Tarchi A., Greve A., Peck A.B., et al. 2004, *MNRAS* 351, 339
- Tinney C.G., Scoville N.Z., & Soifer B.T., 1990, *ApJ* 362, 473
- Trotter A.S., Greenhill L.J., Moran J.M., et al. 1998, *ApJ* 495, 740
- Turner J.L. & Ho P.T.P., 1994 *ApJ* 421, 122
- Usero A., García-Burillo, Fuente A., Martín-Pintado J., & Rodríguez-Fernández N.J., 2004, *A&A* 419, 897
- Vacca W.D., Garmany C.D., & Shull J.M., 1996, *ApJ* 460, 914
- van Dishoeck E.F. & Black J.H., 1988, *ApJ* 334, 771
- Veilleux S., Cecil G., Bland-Hawthorn J., et al. 1994, *ApJ* 433, 48
- Vila-Costas M.B. & Edmunds M.G. 1992 *MNRAS* 259, 121
- Walterbos R.A.M., Braun R., & Kennicutt R.C., 1994, *AJ* 107, 184
- Wilson A.S., & Ulvestad J.S., 1987 *ApJ* 319, 105
- Wilson A.S., Baldwin J.A., Sun S.-D., & Wright A.E., 1986, *ApJ* 310, 121
- Wilson A.S., Helfer T.T., Haniff C.A., & Ward M.J., 1991, *ApJ* 381, 79
- Wynn-Williams C.G., Becklin E.E., & Scoville N.Z., 1985, *ApJ* 297, 607
- Xie S., Young J.S., & Schloerb F.P., 1994, *ApJ* 421, 434
- Young J.S., Claussen M.J., & Scoville N., 1988a *ApJ* 324, 115
- Young J.S., Claussen M.J., Kleinmann S.G., Rubin V.C., & Scoville N.Z., 1988b *ApJL* 331, L81
- Young J.S., Wilson A.S., & Shopbell P.L., 2001 *ApJ* 556, 56
- Young J.S., Xie S., Tacconi L., et al. 1995 *ApJS* 98, 219
- Zaritsky D., Kennicutt R.C. & Huchra J.P., 1994, *ApJ* 420, 87
- Zhao J.-H., Anantharamaiah K.R., Goss W.M., & Viallefond F., 1996, *ApJ* 472, 54